*18 9661*
*p. 16*
*5*

N94-14746

# A small-scale turbulence model

## By T. S. Lundgren[1]

A model for the small-scale structure of turbulence is reformulated in such a way that it may be conveniently computed. The model is an ensemble of randomly oriented structured two dimensional vortices stretched by an axially symmetric strain flow. The energy spectrum of the resulting flow may be expressed as a time integral involving only the enstrophy spectrum of the time evolving two-dimensional cross section flow, which may be obtained numerically. Examples are given in which a $k^{-5/3}$ spectrum is obtained by this method without using large wavenumber asymptotic analysis. The $k^{-5/3}$ inertial range spectrum is shown to be related to the existence of a self-similar enstrophy preserving range in the two-dimensional enstrophy spectrum. The results are insensitive to time dependence of the strain-rate, including even intermittent on-or-off strains.

## 1. Introduction

One of the issues in turbulence theory is to understand what kinds of elementary flow structures are responsible for the part of the turbulent energy spectrum described by Kolmogorov's celebrated $k^{-5/3}$ law. A number of years ago, Lundgren (1982) proposed a model of the small scale structure of turbulence which gives this spectrum. The model was put together as an ensemble of randomly oriented vortices with spiral structure, each vortex being subjected to an axially symmetric irrotational straining field. The strain was made constant and axially symmetric for analytical reasons and this should be thought of as a representation of much more complicated strains. The idea was to model the most important property of turbulence, namely the mixing property which causes fluid particles to rapidly separate, stretching vortex blobs into elongated tubes. This model generalizes an earlier model by Townsend (1951) which assumed randomly oriented Burgers vortices and gave a $k^{-1}$ spectrum.

Differential rotation in the vortices (the inner part has higher angular velocity therefore winds faster) causes the vortex layers in the spiral to tighten, and the axial straining decreases the cross section of the structure. These mechanisms cause a cascade to smaller scales which differs from the traditional concept of a cascade through eddies of different sizes induced by instabilities.

Many turbulent flows have distinct two dimensional vortices, and often flow visualization by laser-induced-fluorescence or smoke shows vortex cross sections with some spiral structure. Such structures may be seen in sections 4 and 6 of Van

1 Department of Aerospace Engineering and Mechanics, University of Minnesota

Dyke's (1982) book. Schwarz (1990) identified intermittently occurring layered vortex sheets (apparently spirals) in oscillating grid turbulence by flow visualization with small suspended crystalline platelets. On the other hand, the numerically simulated periodic box turbulence of Vincent and Meneguzzi (1991) contains very pronounced two-dimensional vortices in which very little internal structure can be seen. (However, there is *some* spiral structure in their figure 15.) Perhaps the Reynolds number is too small in this kind of flow.

A number of authors have made further studies based on the original paper by Lundgren. In particular, Lundgren (1985) applied the model to the calculation of the scalar spectrum of the product of a fast chemical reaction. Gilbert (1988) used similar ideas for the study of two-dimensional turbulence. Buntine and Pullin (1988) and Pullin and Buntine (1989) used the model as a basis for computations of spectra produced by the merger of vortices. Pullin and Saffman (1992) used it to calculate vorticity and velocity derivative moments for homogeneous isotropic turbulence. Recently, Gilbert (1992) has produced a qualitative cascade argument based on the model to explain the Kolmogorov spectrum.

In section 2, the model is reformulated in such a way that the two-dimensional part of the model, the spiral flow or some more general two-dimensional vortical flow, may be conveniently carried out numerically.

In section 3 numerical computations of two-dimensional flows are used to generate three-dimensional energy spectra.

## 2. Reformulation of the spiral vortex model

It will be useful to separate the strictly two-dimensional part of the model, the flow in the cross section of the vortex, from the straining part of the model which is performed by a transformation. The 1982 paper will be referred to as L and equations from that paper will be referred to by L:( ). It was shown in L that if a two-dimensional flow with vorticity given by $\omega_2(x, y, t)$ is placed in an axially symmetric strain flow with velocity components $(-.5ax, -.5ay, az)$ where the strain-rate $a$ may be a function of time, then the vorticity in the resulting three-dimensional flow (which has the same initial vorticity as the two-dimensional flow) is given by

$$\omega(x, y, t) = S(t)\, \omega_2\left(S(t)^{1/2}x, S(t)^{1/2}y, T(t)\right) \tag{2.1}$$

where

$$S(t) = \exp\left(\int_0^t a(t')dt'\right) \tag{2.2}$$

is the amount the flow is stretched and

$$T(t) = \int_0^t S(t')dt' \tag{2.3}$$

is a strained time. The energy spectrum of an ensemble of strained vortices of all ages, accounting for the greater length of the older vortices, may be deduced from L:(58), L:(75) and L:(76) and expressed, in a new form, by

$$E(k) = \frac{C}{k^2} \int_0^{T_c} S(T)^{1/2} F_2\left(S(T)^{-1/2}k, T\right) dT \tag{2.4}$$

where $C = 2\pi^2 l_0 N_c / L^3$ is a constant. The function $F_2$ is the enstrophy spectrum (the vorticity power spectrum) of the strictly two-dimensional flow. This is defined by

$$F_2(k,t) = k \int_0^{2\pi} |\bar{\omega}_2(k\cos\theta_k, k\sin\theta_k, t)|^2 d\theta_k \tag{2.5}$$

where

$$\bar{\omega}_2 = \frac{1}{(2\pi)^2} \int\int \exp\left[-i(k_x x + k_y y)\right] \omega_2(x,y,t) dx dy \tag{2.6}$$

and represents the enstrophy in a circular shell in wavenumber space, divided by the width of the shell. The integration variable in Eq.(2.4) is the strained time and the stretching function $S$ must be expressed as a function of this strained time. When the strain-rate is constant, the usual case considered, $S = \exp(at)$ and $T = (\exp(at) - 1)/a$ and hence

$$S = 1 + aT \tag{2.7}$$

is the appropriate function. In appendix A, it is shown by example that, even when the strain-rate is variable and quite different from constant, the stretching function is roughly a linear function of the strained time and the energy spectrum computed from Eq.(2.4) is insensitive to these modest deviations from linearity.

In Eq.(2.4), the function $F_2$ is all that is needed from the two-dimensional flow, and it may be specified numerically or analytically. The time integral represents the effect of stretching. The finite time cut-off on the integral is to prevent the vortices from being stretched indefinitely. It was assumed in L that they ultimately coalesce into shorter vortices and renew the spiral structure.

In L an analytical spiral vortex solution was developed. An approximate solution of the two-dimensional Navier-Stokes equation was given in the form of a Fourier series in the cylindrical angle variable $\theta$,

$$\omega(r,\theta,t) = \sum_{n=-\infty}^{\infty} \omega_n(r,t) \exp(in\theta) \tag{2.8}$$

$$\omega_n(r,t) = f_n(r) \exp\left[-in\Omega(r)t - \frac{1}{3}n^2 \left(\frac{d\Omega}{dr}\right)^2 \nu t^3\right] \tag{2.9}$$

where the functions $f_n$ are arbitrary and the angular velocity $\Omega(r)$ is related to the average vorticity $\omega_0$ by

$$r\omega_0 = \frac{d}{dr}r^2\Omega(r). \tag{2.10}$$

The function $\Omega(r)$ must be monotone decreasing – the property which gives differential rotation. If the functions $f_n$ are all the same (independent of $n$) the solution looks like a spiraling vortex sheet in the inviscid limit. The approximations in Eq.(2.8) require that $t$ must be large, i.e., the error becomes small as $t \to \infty$. However, it will be seen numerically that it is quite good even for fairly small $t$.

By using this analytical solution, the enstrophy function $F_2$ may be expressed as a series of integrals which involve Bessel functions. These may be evaluated by the method of stationary phase, which requires both $k$ and $t$ to be large, an asymptotic result which may be written

$$F_2 = t^{-1} G(k/t) \exp(-2\nu k^2 t/3) \tag{2.11}$$

where

$$G(k/t) = \frac{1}{\pi} \sum_{n=1}^{\infty} \frac{r_n}{n\Omega''(r_n)} |f_n(r_n)|^2 \tag{2.12}$$

with

$$k + n\Omega'(r_n)t = 0. \tag{2.13}$$

The last equation results from the method of stationary phase. One is supposed to solve this for $r_n$ and substitute it into Eq.(2.12). Note that $r_n$ is a function of $k/t$, hence the form of the argument of the function $G$. In writing this result, the contribution from the $n = 0$ term has been omitted. This term has a different functional dependence and was shown in L to contribute little at high wavenumber. Equation (2.11) does not appear in L but may be deduced from L:(66) and L:(64) (with $S \equiv 1$ and $P \equiv t$).

It is the functional form of Eq.(2.11) which is important. First note that the functions $f_n$ are assumed to be of limited extent so that the spiral is restricted to a halo around a central vortex. Then the function $F_2$ looks like a localized hump when plotted versus wavenumber (this will be clear when some computations are seen). If the viscous factor can be neglected, the area under the hump stays constant because

$$\int_0^{\infty} t^{-1} G(k/t) \, dk \equiv \text{constant}. \tag{2.14}$$

The similarity form of the function shows that the top of the hump moves to higher wavenumber with constant speed, while the width broadens and the peak decreases in such a way that the area stays constant. This is an enstrophy preserving temporal cascade. The physics is clear: as the spiral turns tighten due to differential rotation, the enstrophy shifts to higher wavenumber while being conserved.

The function $F_2$ given by Eq.(2.11) is only part of the enstrophy spectrum. There is an additional large part at low wave number (the $n = 0$ term which was omitted). If viscosity is neglected, the *total* enstrophy is preserved, i.e., $\int \omega_2^2 dA = \int F_2 dk \equiv$ constant. What has been shown here is that the spiral solution has scale separation of the enstrophy spectrum into two distinct peaks, and the enstrophy of each of these parts is independently preserved.

The energy spectrum expression given by Eq.(2.4) could also have been cast in terms of the two-dimensional energy spectrum, $E_2$ say. For the spiral solution, $E_2$ also has scale separation into a large low wavenumber peak and a secondary smaller (much smaller because of the $k^{-2}$ factor) high wave number peak with a similarity structure. While the total energy is conserved (in the absence of viscosity), the

energy in the separate peaks is not. The energy in the high wavenumber peak decreases like $t^{-2}$, giving up this energy to the low wavenumber peak.

This enstrophy preserving similarity form is responsible for the $k^{-5/3}$ part of the three-dimensional energy spectrum. When Eq.(2.11) is substituted into Eq.(2.4), the result

$$E(k) = Ak^{-5/3}\exp(-2\nu k^2/3a) \tag{2.15}$$

is obtained if one takes the upper limit to be infinite and approximates Eq.(2.7) by $S \simeq aT$, i.e., most of the contribution to the integral comes from large values of $S$. Equation (2.15) results from a simple change of the integration variable to $T/k^{2/3}$ and doesn't depend at all on the specific form of $G$. This generalizes the model since there could be other kinds of flows with scale-separated self-similar conservative enstrophy spectra, although none are presently known.

The following qualitative derivation of the functional form of the enstrophy spectrum was motivated by a discussion with Javier Jimenez. *Assume* that the enstrophy spectrum has a self-similar form $t^{-\alpha}G(k/t^\beta)$, then it is easy to see that conservation of enstrophy implies $\alpha = \beta$. One may argue that in a fairly steady shear flow the length of an element of a vortex sheet increases linearly with $t$; its thickness, therefore, decreases like $t^{-1}$. The largest wavenumber in a system of such vortex sheets behaves like the reciprocal of the thickness. Therefore, $k \sim t$ and $\alpha = \beta = 1$, as desired.

It can also be noted that if there is no axial straining, so that $S \equiv 1$, Eq.(2.4) and Eq.(2.11) (without the viscous part) gives

$$E(k) \sim k^{-2}. \tag{2.16}$$

This was also noted by Gilbert (1988) and is consistent with Townsend's (1951) observation that a $k^{-2}$ spectrum results from random arrays of vortex sheets. The conclusion to be drawn is that the axial straining gives the extra $k^{1/3}$.

The integration in Eq.(2.4) may be understood as follows. Imagine a $K, T$ plane with $S^{1/2}F_2(K,T)$ plotted in a third dimension. This function looks like a ridge centered along a ray from the origin of the $K, T$ plane, decreasing in height and spreading for increasing $T$. The argument $K = S^{-1/2}k$ required in Eq.(2.4) is a curve in the $K, T$ plane starting from $K = k$ at $T = 0$ and moving to smaller $K$ for larger $T$. The integrand in Eq.(2.4) is the height of the ridge seen as one traverses this curve. In order to get $k^{-5/3}$ for a band of $k$-values, the integration must extend through the ridge into the small values on the far side, for all $k$-values in this band.

## 3. Computations

The formula expressed by Eq.(2.4) makes it possible to test some of the analytical limitations of the spiral vortex model, since the two-dimensional enstrophy spectrum may be computed from numerical solutions of the two-dimensional Navier-Stokes equations rather than depending entirely on asymptotic methods. Further, one can use more general two-dimensional solutions. Buntine and Pullin (1988) and Pullin and Buntine (1989) used numerical analysis in a similar context. Their

approach was somewhat different than that described here. They expanded the two-dimensional vorticity in a Fourier series, as in Eq.(2.8), and solved numerically for the coefficients $\omega_n(r,t)$. These functions were then used to evaluate the Bessel function integrals required for L:(60), and finally the energy spectrum was obtained through the appropriate time integration. The advantage of the present approach is flexibility. Having identified the required physical quantity as the two-dimensional enstrophy spectrum, it may be computed by *any* method and processed through Eq.(2.4) without further reference to the detailed analytical expansions of Lundgren (1982).

In the computations reported below, a pseudo-spectral method was employed in a vorticity/streamfunction formulation in a square region with periodic boundary conditions. Aliasing errors were removed by the 2/3 rule and most of the computations were done with $240^2$ resolution. The computations were performed at the Center for Turbulence Research at NASA Ames Research Center on a Cray YMP.

The characteristic length in the flows was taken such that the sides of the box have dimensionless length equal $2\pi$ units; this makes the wavenumbers be integers. The actual *unit* of length was related to some measure of the initial radius of the vorticity distribution, thus the vortex is quite a bit smaller than the box. The characteristic velocity was selected such that the dimensionless circulation of the vortex was unity. This makes the Reynolds number of the flows be $\Gamma/\nu$ where $\Gamma$ is the dimensional circulation of the vortex. The Reynolds number would be about an order of magnitude smaller if an average swirling velocity at unit radius were used for the characteristic velocity. The dimensionless turn around time is about 40 units.

The enstrophy spectrum, given by Eq.(2.5), was approximated by summing all values of the squared magnitudes of the discrete Fourier coefficients with $x, y$ wavenumbers in a cylindrical shell of unit wavelength in wave space. This value is then assigned to a wavenumber which is the midradius of the shell.

Two series of computations were done with the spiral vortex solution. In the first, the two-dimensional enstrophy spectrum was computed from the analytical spiral solution by a fast Fourier transform algorithm. The second computes the enstrophy spectrum from a numerical solution of the spectral equations with the spiral solution as an initial condition. Comparison thus tests the integrity of the spiral solution.

The spiral solution was taken in the form of a two-sided rollup with two halo spirals of amplitude $f$, with 180° separation, plus an additional central core. The specific functions used here are expressed as

$$\omega_2(r,\theta,t) = \omega_0(r) + 2f(r) \sum_{n=1}^{\infty} \cos\left[2n(\theta - \Omega(r)t)\right] \exp\left(-4n^2\Omega'(r)^2\nu t^3/3\right), \quad (3.1)$$

$$\omega_0(r) = \Gamma \, \frac{\exp\left[-(r/a)^2\right]}{(1+h)\pi a^2} + 2f(r), \quad (3.2)$$

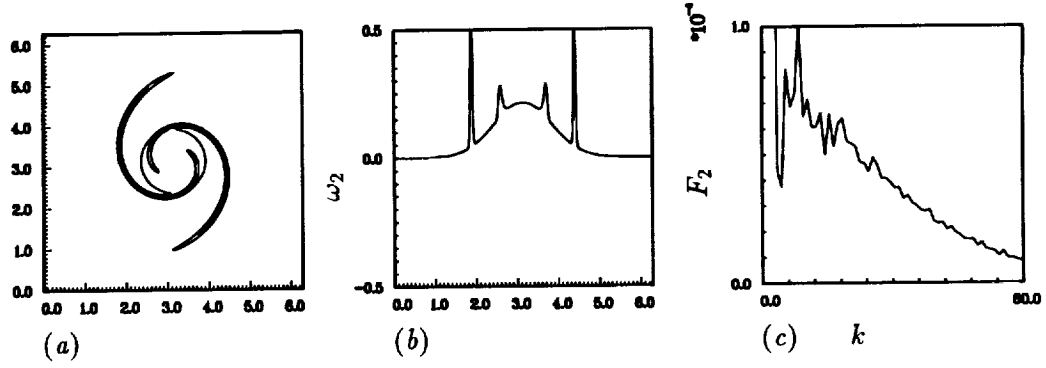$$f(r) = \Gamma \, \frac{h(r/a)^2 \exp\left[-(r/a)^2\right]}{2(1+h)\pi a^2}, \quad (3.3)$$

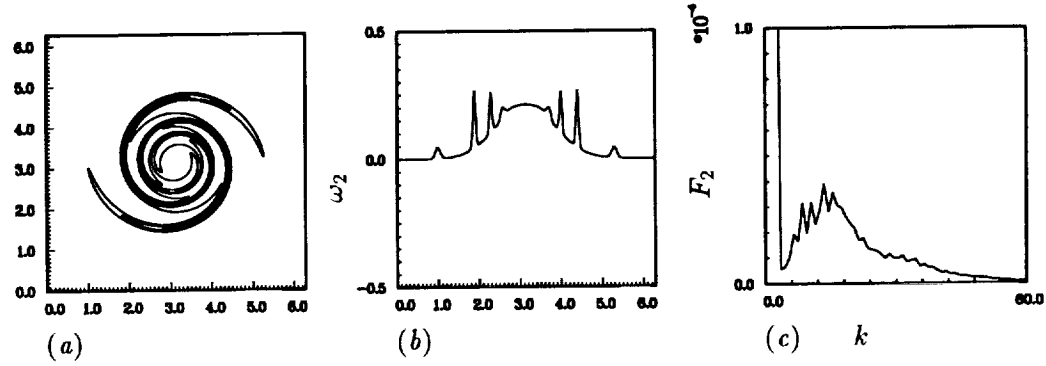FIGURE 1.1.   $t=0$ , $t_{spiral}=50$. See caption below.



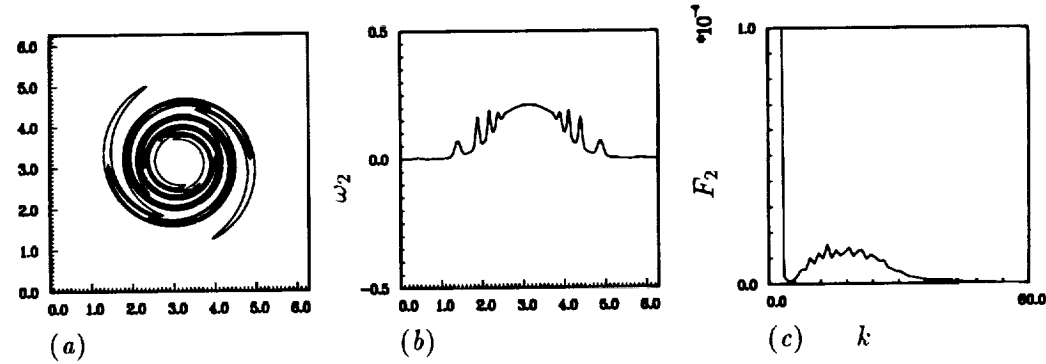FIGURE 1.2.   $t=50$ , $t_{spiral}=100$. See caption below.



FIGURE 1.3.   $t=100$, $t_{spiral}=150$. See caption below.

$$\Omega(r) = \Gamma \; \frac{\left[1 + h - \left(1 + h + h(r/a)^2\right)\exp\left(-(r/a)^2\right)\right]}{2(1 + h)\pi a^2}, \tag{3.4}$$

$$\Omega'(r) = \frac{[\omega_0(r) - 2\Omega(r)]}{r}, \tag{3.5}$$

where $\Gamma$ is the circulation of the vortex, $a$ is a radial dimension and $h$ is a constant. If $0 < h < 1$, $\Omega(r)$ will be monotone decreasing. In dimensionless form $\Gamma = 1$, $a = 1$, $\nu$ is the reciprocal of the Reynolds number and in these computations $h = 1/2$ .
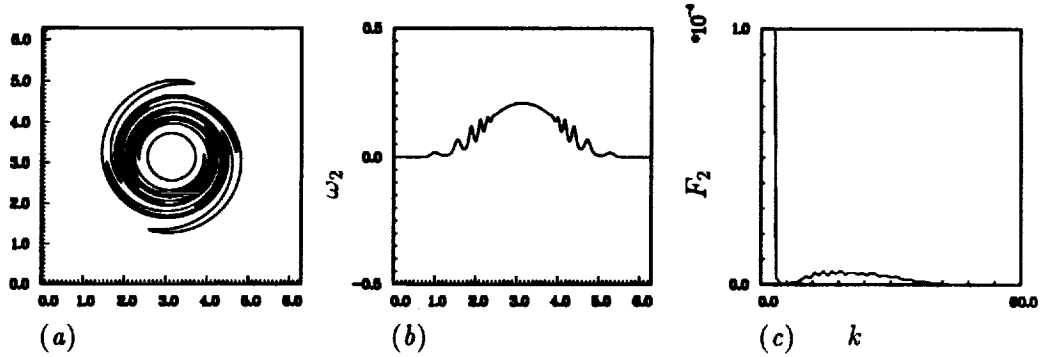
FIGURE 1.4.   $t{=}150$, $t_{\text{spiral}}{=}200$. See caption below.
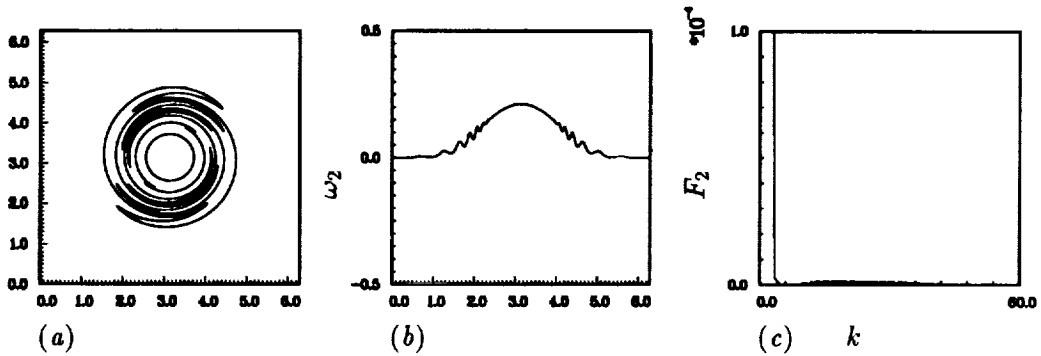
FIGURE 1.5.   $t{=}200$, $t_{\text{spiral}}{=}250$. See caption below.

FIGURE 1.1–1.5.   Analytical spiral solution at selected times. $t_{\text{spiral}}$ is the time in Eq.(3.1), $t$ is for comparison with figures (2.1)–(2.5) which have the same initial condition. $\Gamma/\nu = 25{,}000$. ($a$) vorticity contours. ($b$) vorticity along a horizontal cut through the middle of ($a$). ($c$) Enstrophy spectrum versus wavenumber.
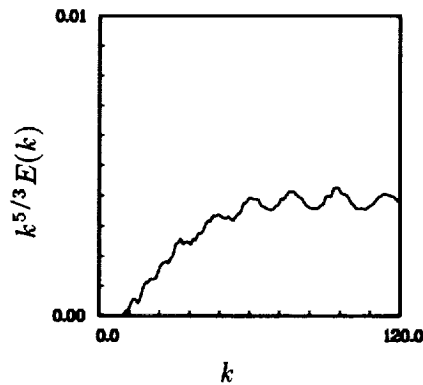
FIGURE 1.6.   $k^{5/3}$ times the three-dimensional energy spectrum calculated by using Eq.(2.4) with the analytical spiral solution.
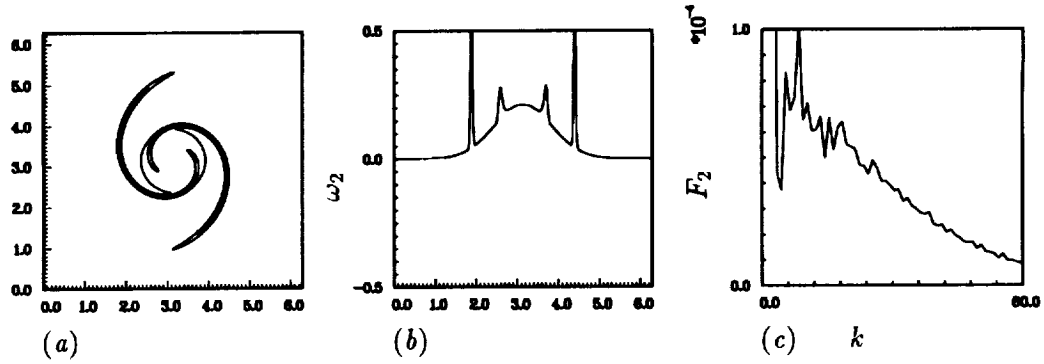
FIGURE 2.1. *t*=0. See caption below.
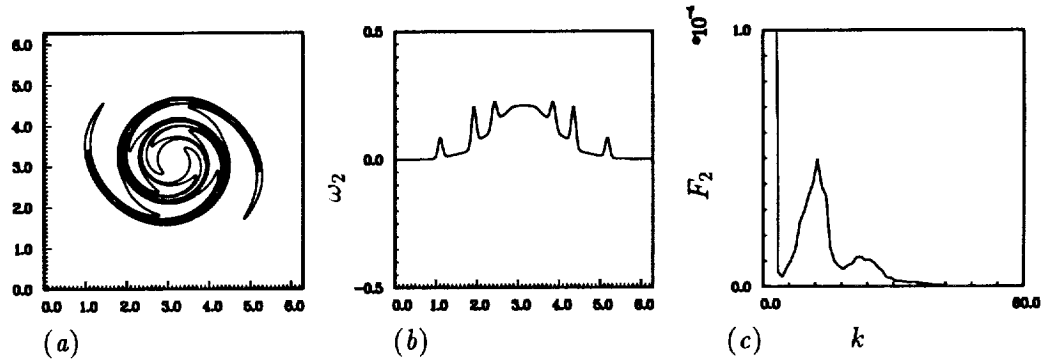


FIGURE 2.2. *t*=50. See caption below.
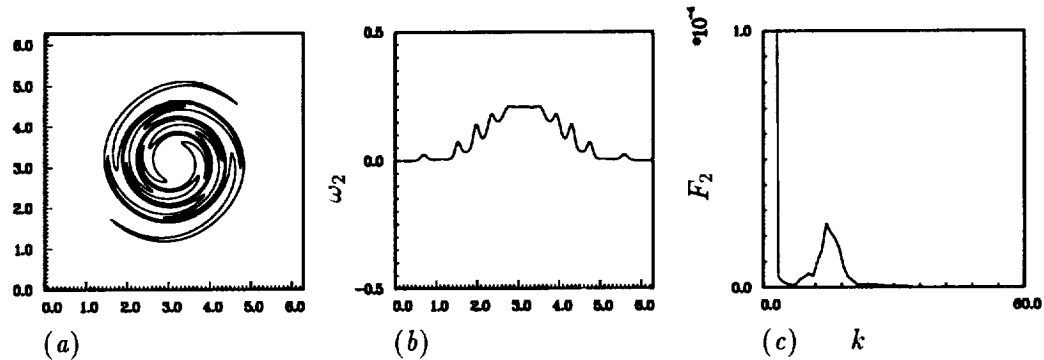


FIGURE 2.3. *t*=100. See caption below.

The first series, displayed in figures 1.1–1.6, is computed from the analytical solution with $\Gamma/\nu = 25,000$. The required discrete Fourier series were computed by means of Temperton's fast Fourier transform algorithms. The figures labeled ($a$) are vorticity contours at 5 times starting with the partially wound state corresponding to a dimensionless time $t_{\mathrm{spiral}} = 50$; the figures labeled ($b$) show the vorticity along a horizontal cut through the middle of the contour figures. The figures labeled ($c$) are of the enstrophy spectrum. There is a huge peak at low wavenumber which is off scale in these figures. Enstrophy similarity, which was found asymptotically,
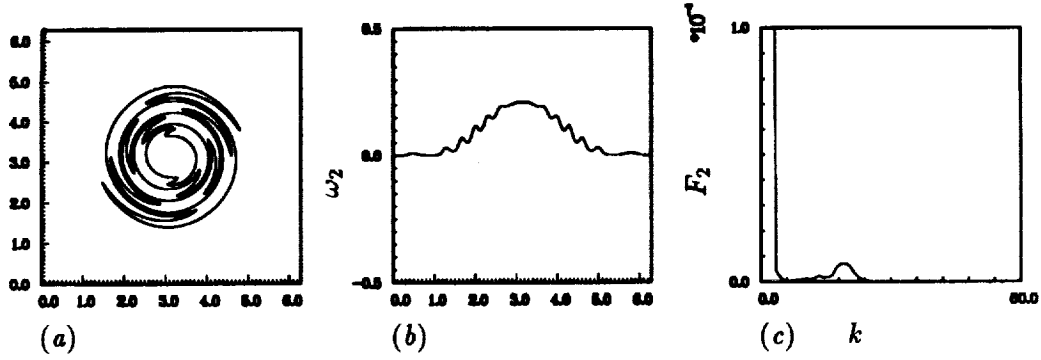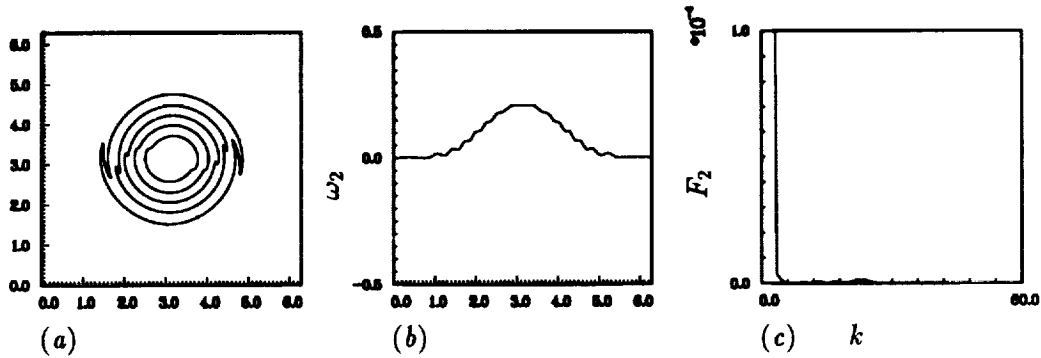
FIGURE 2.4. $t=150$. See caption below.



FIGURE 2.5. $t=200$. See caption below.

FIGURE 2.1–2.5. Computed spiral solution at selected times. $\Gamma/\nu = 25,000$. (a) vorticity contours. (b) vorticity along a horizontal cut through the middle of (a). (c) Enstrophy spectrum versus wavenumber.
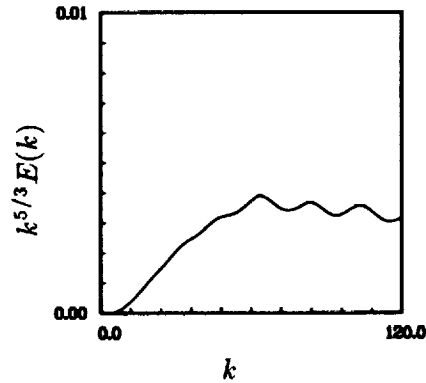


FIGURE 2.6. $k^{5/3}$ times the three-dimensional energy spectrum calculated by using Eq.(2.4) with solution computed using the analytical spiral solution as initial condition.
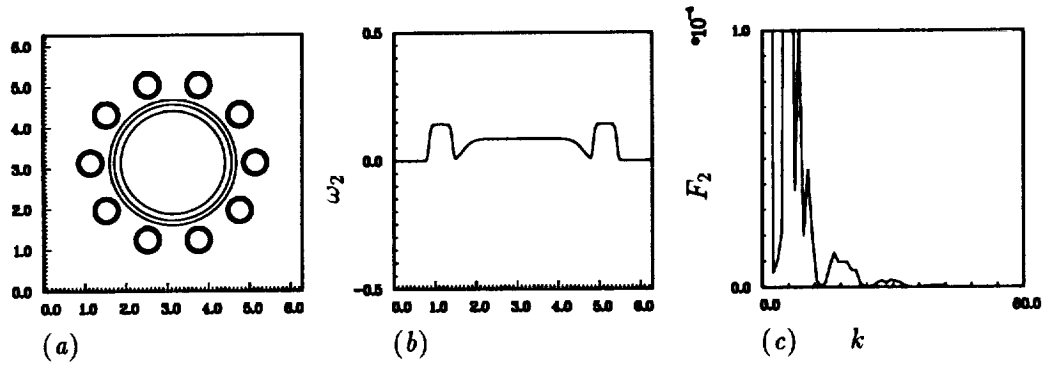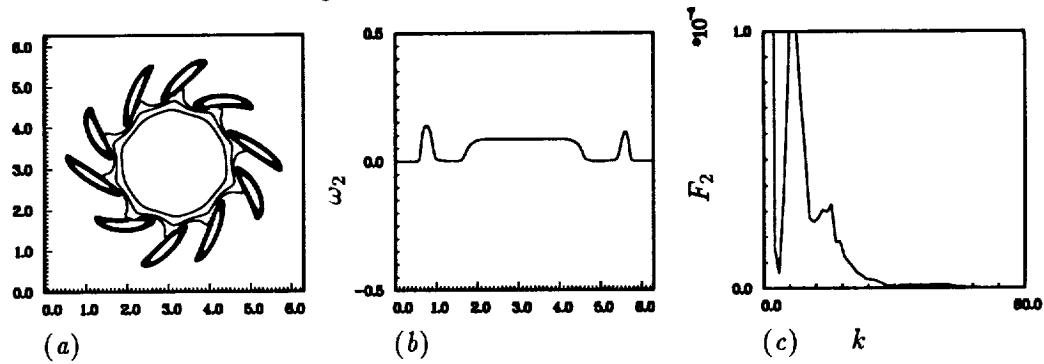
FIGURE 3.1. $t=0$. See caption below.
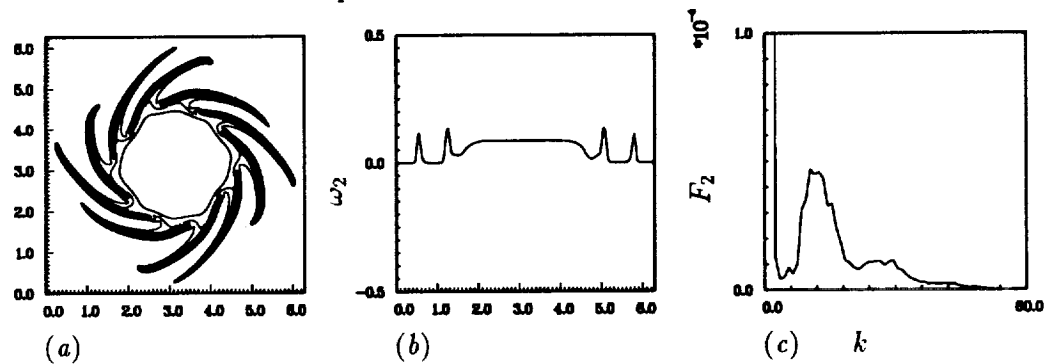
FIGURE 3.2. $t=50$. See caption below.

FIGURE 3.3. $t=100$. See caption below.

is not perfect but is qualitatively recognizable. As time increases, one can see the number of turns in the spiral increase due to differential rotation and the peak in the enstrophy spectrum move outward to larger wavenumber as the spatial scale in the spiral decreases.

Figure 1.6 shows the three-dimensional energy spectrum computed from Eq.(2.4). The integration was carried out from $T = 0$ to $T = 250$ with a coarse integration time interval of $\Delta T = 5$, which was adequate here. (In computations where the Navier-Stokes equations were solved numerically, $\Delta T$ was taken the same as the
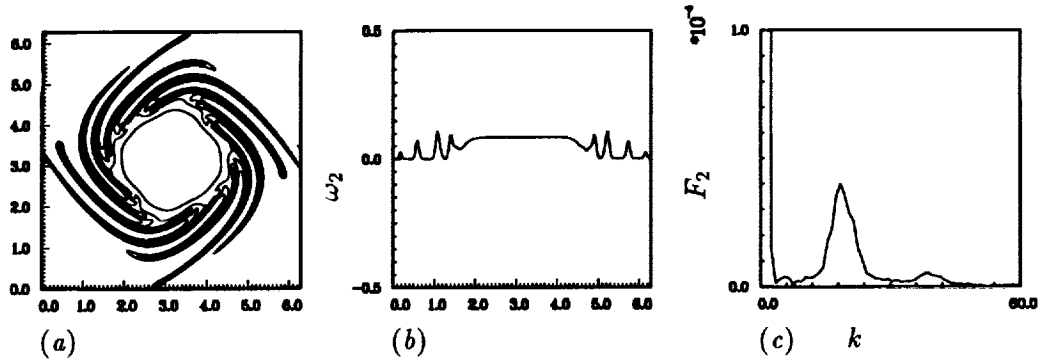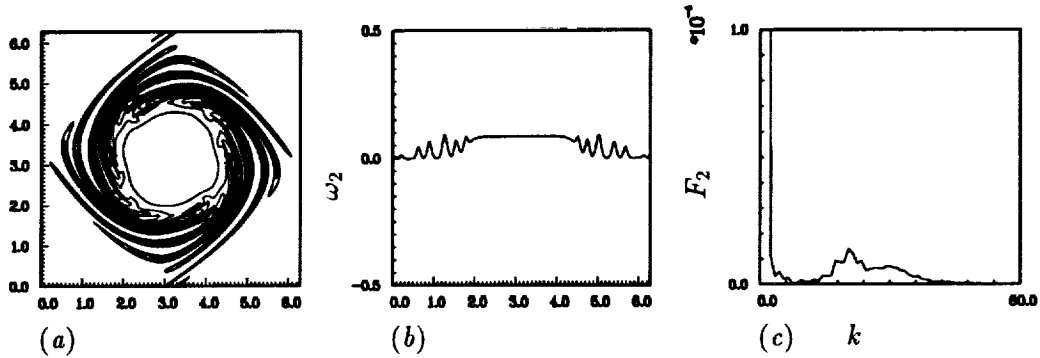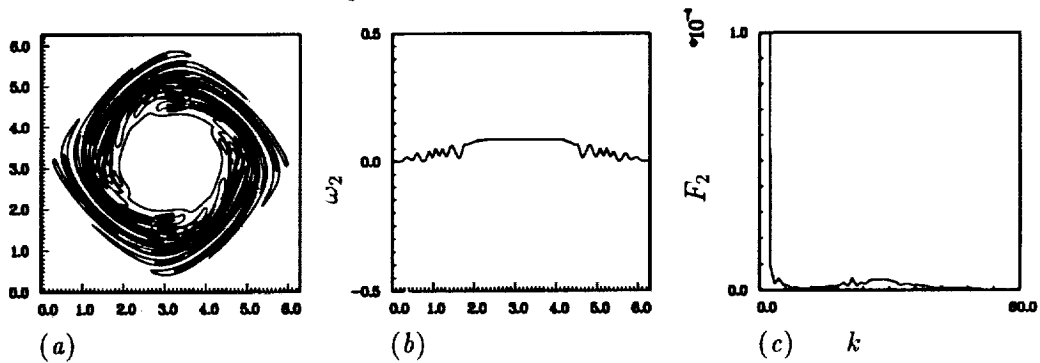
FIGURE 3.4.  $t$=150. See caption below.

FIGURE 3.5.  $t$=200. See caption below.

FIGURE 3.6.  $t$=250. See caption below.

FIGURE 3.1—3.6.  Computed spiral solution at selected times. $\Gamma/\nu = 100,000$. ($a$) vorticity contours. ($b$) vorticity along a horizontal cut through the middle of ($a$). ($c$) Enstrophy spectrum versus wavenumber.

updating time step, namely $\Delta T = .05$.) The strain-rate was taken to be unity. The low wavenumber end of the spectrum was suppressed by cutting off the integration when $S(T)^{-1/2}k$ is less than 5, thus avoiding the large low wavenumber enstrophy peak. The result in figure 1.6 has a wavenumber range from about 60 to 120 where
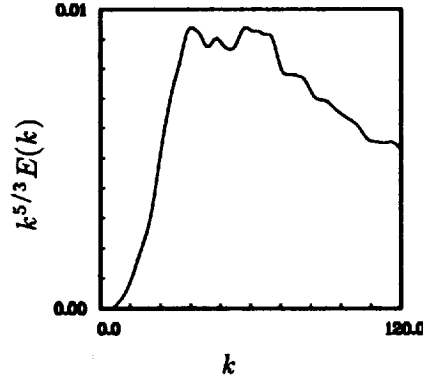
FIGURE 3.7. $k^{5/3}$ times the three dimensional energy spectrum calculated by using Eq.(2.4) with the solution depicted in figures 3.1– 3.6.

the spectrum is approximately $k^{-5/3}$. Note that since $2^{1/3} \simeq 1.26$, one should be able to tell the difference between $k^{-5/3}$ and $k^{-2}$ on this figure.

The second series of computations, seen in figures 2.1–2.6, are presented in the same format as the first series. The Navier-Stokes equations were solved numerically with initial conditions the same as the initial frame of the first series. Here the object is to show that the analytical spiral solution is a good approximation to the Navier-Stokes equations even though time ($t_{\text{spiral}}$) is not large enough at the beginning for the spiral to have many turns. Comparing the two series of computations, one can see that the results are quite close but not identical. In particular the enstrophy spectrum of the second series is smoother and more compact. The energy spectrum is very similar but perhaps slightly tipped toward $k^{-2}$.

A third series of computations has been carried out with quite different initial conditions with the objective of producing a spiral solution without actually starting with one. The vorticity distribution at the initial time is shown in figure 3.1. One large vortex, with radius 1.5, almost uniform vorticity and circulation .6 is surrounded by 10 smaller vortices with centers 2 units from the center of the large vortex. Each of these smaller vortices have radii .3 units and circulation .04 so that the total circulation of the configuration is unity. The Reynolds number was $\Gamma/\nu = 100,000$. The smaller vortices get sheared into bands of vorticity which continue to tighten in the differential rotation of the combined vorticity. The result is a multilayered spiral vortex with a decent enstrophy cascade. Similarity is approximately satisfied; comparing the enstrophy spectrum at $t = 50$ with that at $t = 100$, the amplitude is almost half and the peaks have moved approximately to twice the wavenumbers as required by similarity. However, comparison of $t = 100$ with $t = 200$ is not quite as satisfactory.

The energy spectrum in figure 3.7 has a short $k^{-5/3}$ range from about $k = 36$ to $k = 72$ and then falls off faster. The viscous factor in Eq.(2.15), which is about .9 when $k = 120$, is not small enough to account for all of the observed decrease.

## 4. Conclusions

The original 1982 spiral vortex model was reformulated in a form where the effect of the two-dimensional flow in the vortex cross section was more clearly separated from the axial stretching. While this was done in order to be able to use computational methods more effectively, the new formulation has allowed greater insight into the workings of the model. It was shown in section 1 that, in the inviscid limit, the analytical spiral vortex solution gives an asymptotic time-dependent enstrophy spectrum in a self-similar form which conserves enstrophy. It is this self-similar form which leads to the $k^{-5/3}$ energy spectrum.

Computations with flows which develop spiral structure showed, qualitatively correct, but imperfect, self-similar enstrophy spectra. The resulting three-dimensional energy spectra nevertheless showed short ranges with the $k^{-5/3}$ power law. These results seem quite rugged and verify results which were previously obtained asymptotically.

The integral which processes the computed two-dimensional enstrophy spectrum to produce the three-dimensional energy spectrum requires integrations over a very long times, of the order of 6 turn-around-times, during which the vortex is stretched by a factor of about 250. The result from appendix A, which shows that the strain may be applied intermittently, make this seem more reasonable.

## Acknowledgements

## Appendix A. Insensitivity to time dependent strain-rate

The strain-rate which a real vortex feels is generated by the presence of other nearby vortices and is unlikely to be constant for very long; therefore, it is important to see if the results are sensitive to time dependence of the strain-rate function.

Equation (2.4) calls for the stretching function $S$ to be expressed as a function of the strained time $T$. When the strain-rate $a(t)$ is constant this leads to the simple linear relationship given by Eq.(2.7). When the strain-rate is not constant, $S$ and $T$ are defined by

$$S(t) = \exp\left(\int_0^t a(t')dt'\right) \tag{A1}$$

$$T(t) = \int_0^t S(t')dt' \tag{A2}$$

and it is not simple to relate them analytically, though it is clear that since $S$ is positive, $T$ is a strictly increasing function of time which can be inverted in principle. It is easy to get the relationship numerically in special cases. As an example, the strain-rate function

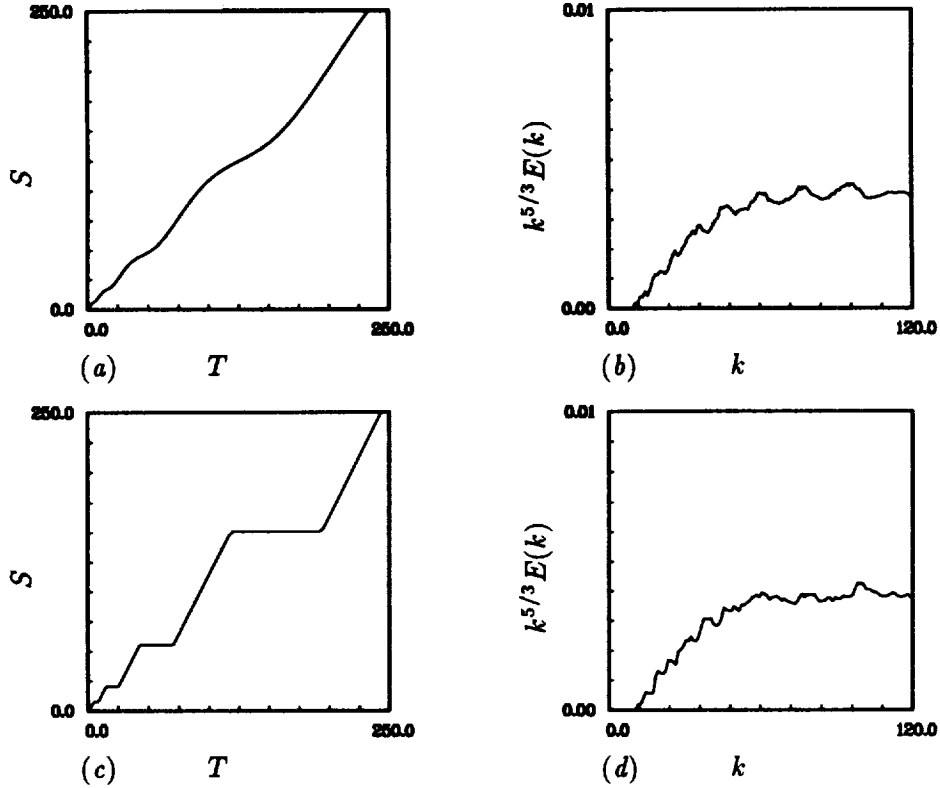$$a(t) = 1 + .5\sin(2\pi t) \tag{A3}$$

FIGURE 4.   Time dependent strain-rate. $(a),(b)$ generated with sinusoidal strain-rate, $a(t) = 1 + .5\sin(2\pi t)$; $(c),(d)$ generated with on-off strain-rate of same period, $a(t) = 1 + (-1)^{\mathrm{int}(2t)}$ .

has average value unity and periodic variations of $\pm 50\%$. During each successive period, the stretch increases by a factor $e$. These functions have been computed (by solving the pair of differential equations $dS/dt = aS$, $dT/dt = S$) and presented as $S$ vs. $T$ in figure 4a. The relationship is roughly linear. This function was used in Eq.(2.4) to compute the energy spectrum using the analytical spiral solution with the same set-up as for the "series one" computations. The resulting energy spectrum in figure 4b is almost identical with that in figure 1.6 which had constant strain-rate. Therefore, it appears that the spectral results are insensitive to moderate variations in strain-rate.

A more extreme intermittent case was tried in which there are alternating periods of positive strain-rate and zero strain-rate. The function used was

$$a(t) = 1 + (-1)^{\mathrm{int}(2t)} \tag{$A4$}$$

where the function "int" truncates the decimal part of a number. This strain-rate function has the same period as Eq.(A3) and the same average value. Alternating half-periods have $a = 2$ or $a = 0$. The $S$ vs. $T$ result in figure 4c is still very roughly linear, and the energy spectrum still has the same range of $k^{-5/3}$.

As one increases the frequency of the strain-rate function, the relationship between $S$ and $T$ will become more nearly linear and will have little effect on the spectral result. Lower frequencies could have an effect. In the extreme case of very long on and off periods, one would get either $k^{-5/3}$ or $k^{-2}$, depending on which period comes first.

## REFERENCES

BUNTINE, J. D. & PULLIN, D. I. 1988 Merger and cancellation of strained vortices. *J. Fluid Mech.* **205**, 263.

GILBERT, A. D. 1988 Spiral structures and spectra in two-dimensional turbulence. *J. Fluid Mech.* **193**, 475.

GILBERT, A. D. 1992 A cascade interpretation of Lundgren's stretched spiral vortex model for turbulent fine structure. Private communication.

LUNDGREN, T. S. 1982 Strained spiral vortex model for turbulent fine structure. *Phys. Fluids* **25**, 2193.

LUNDGREN, T. S. 1985 The concentration spectrum of the product of a fast bimolecular reaction. *Chem. Eng. Sci.* **40**, 1641.

PULLIN, D. I. & BUNTINE, J. D. 1989 Interactive dynamics of strained vortices. *Tenth Australian Fluid Mechanics Conference–University of Melbourne*, 9.5.

PULLIN, D. I. & SAFFMAN, P. G. 1992 On the Lundgren-Townsend model of turbulent fine scales. Submitted for publication.

SCHWARZ, K. W. 1990 Evidence for organized small-scale structure in fully developed turbulence. *Phys. Rev. Lett.* **64**, 415.

TOWNSEND, A. A. 1951 On the fine-scale structure of turbulence. *Proc. Roy. Soc. Lond.* **A 208**, 534.

VAN DYKE, M. 1982 *An Album of Fluid Motion.* Stanford, Parabolic Press.

VINCENT, A. & MENEGUZZI, M. 1991 The spatial structure and statistical properties of homogeneous turbulence. *J. Fluid Mech.* **225**, 1.